

# Low-Leakage High-Breakdown Laterally Integrated HEMT-LED via n-GaN Electrode

Chao Liu, Yuefei Cai, Xinbo Zou, *Member, IEEE*, and Kei May Lau, *Fellow, IEEE*

**Abstract**—We report lateral integration of an InGaN/GaN light-emitting diode (LED) and an AlGaN/GaN high electron mobility transistor (HEMT) via the epitaxial layers. Direct contact of the HEMT channel and the n-GaN electrode of the LED allows for conversion of a current-controlled LED to a voltage-controlled device by the gate and drain biases. The integrated HEMT-LED exhibited a light output power of 7 mW from the LED with a modulated injection current of 80 mA through the HEMT ( $V_{DD} = 8$  V and  $V_{GS} = 1$  V). The off-state breakdown voltage for the integrated HEMT-LED was 530 and 270 V at forward and reverse bias condition, respectively. The superior characteristics are attributed to the common GaN/AlN buffer platform featured with high crystalline quality and large resistivity simultaneously.

**Index Terms**—Light emitting diodes, high electron mobility transistors, monolithic integration.

## I. INTRODUCTION

COMPARED to traditional incandescent and fluorescent lamps, InGaN/GaN light emitting diodes (LEDs) exhibit high luminous efficiency, long lifetime, and environmentally friendly characteristics. These superior properties render them promising building blocks in smart lighting and display systems. To allow for flexible driver design compatible with conventional power ICs, voltage-controlled LEDs are simpler to work with.

Integration at the component level is an important approach to achieve such a voltage-controlled device. There are two commonly adopted integration strategies: hybrid integration at the package level and monolithic integration at the chip level. Monolithic integration of GaN photonic and electronic devices can simplify the packaging complexity and reduce parasitic components in realizing a smart lighting system [1], [2]. GaN-based devices have shown superior performance such as low on resistance, low capacitance, and high operating frequency, making them good candidates for power amplifier and switch mode power supply applications [3]. Further miniaturization of GaN power devices and integration with GaN LEDs are desirable and can be enabled by sharing the same

Manuscript received January 26, 2016; revised February 17, 2016; accepted February 17, 2016. Date of publication February 24, 2016; date of current version March 29, 2016. This work was supported by the Research Grants Council, Hong Kong, under Grant 16204714 and Grant T23-612/12-R.

The authors are with the Department of Electronic and Computer Engineering, The Hong Kong University of Science and Technology, Hong Kong (e-mail: eekmlau@ust.hk).

Color versions of one or more of the figures in this letter are available online at <http://ieeexplore.ieee.org>.

Digital Object Identifier 10.1109/LPT.2016.2532338

material platform. Recently, Li *et al.* [4], [5] and Lee *et al.* [6] reported monolithic HEMT-LED integration by selective epi removal (SER) of vertically stacked epitaxial structures. However, difficulties in controlling the etching depth and the associated plasma damage during dry etching significantly degraded the performance of the transistors. We utilized an alternative integration scheme by selective area growth (SAG) technique, as reported in [7] and [8]. Our initial approach was an HEMT-on-LED scheme featuring a high brightness LED underneath the HEMT. This configuration led to a highly leaky HEMT grown on top of the conductive p-type GaN underneath (contact layer of the LED) and resulted in poor isolation by the thin regrown buffer [9]. To improve the leakage characteristics and reduce the interconnect parasitics, we developed a new lateral integration scheme, in which the n-type GaN electrode of the LED formed an in-situ contact with the GaN channel of the HEMT during the SAG of the LED structure [10]. As a result, no extra metal-interconnect was needed and the interconnect parasitics were reduced effectively. The integrated HEMT-LED is a three-terminal light-emitter controlled by the gate and drain biases of the HEMT.

The major challenge of the lateral scheme is to obtain a common buffer layer optimized for both the LED and the HEMT. When growing a GaN buffer on sapphire, using a low temperature (LT) GaN nucleation layer always leads to a trade-off between the crystalline quality and buffer resistivity, as found in [11] and [12]. Despite of its superior crystalline quality, the high quality (HQ) GaN buffer widely adopted for LED growth on sapphire suffers from a high buffer leakage, which is undesirable for the HEMT part. In our previous work, the brightness of the LED was compromised to insure a low leakage HEMT, when the high resistance (HR) GaN buffer on sapphire was adopted. In this work, we have developed a GaN/AlN buffer on sapphire which features good crystalline quality and high buffer resistivity simultaneously. The integrated HEMT-LED on the GaN/AlN buffer exhibited improved brightness and reduced leakage.

## II. DEVICE STRUCTURE AND FABRICATION

The AlGaN/GaN HEMT structure used in this work was grown on a 2-inch sapphire substrate in an Aixtron 2400HT metal organic chemical vapor deposition (MOCVD) system. Trimethylgallium (TMGa), trimethylaluminum (TMAI) and ammonia ( $\text{NH}_3$ ) were used as Ga, Al and N sources, respectively. Nitrogen and hydrogen were used as carrier gas. From bottom to top, the AlGaN/GaN HEMT structure consisted of a 150 nm AlN nucleation layer, a 3  $\mu\text{m}$  GaN

TABLE I  
COMPARISON OF DIFFERENT BUFFER STRUCTURES ON SAPPHIRE

Buffer	FWHM (002) /arcsec	FWHM (102) /arcsec	TD density /cm <sup>2</sup>	Leakage /nA
GaN/AlN buffer	238	321	$3.2 \times 10^8$	21
HR GaN buffer	313	688	$1.3 \times 10^9$	28
HQ GaN buffer	297	330	$3.6 \times 10^8$	>1000

buffer, a 100 nm unintentionally doped GaN channel layer, a 1 nm AlN spacer layer, and a 20 nm  $\text{Al}_{0.3}\text{Ga}_{0.7}\text{N}$  barrier layer. The optimal AlN nucleation layer used in this work was grown at 1150 °C, 50 mbar and a V/III of 500. Van der Pauw measurements for the as-grown AlGaN/GaN HEMT structure using the GaN/AlN buffer showed a sheet resistance ( $R_s$ ) of 280 Ω/sq, with a Hall mobility of 1810 cm<sup>2</sup>/V·s and a sheet carrier concentration of  $1.2 \times 10^{13} \text{ cm}^{-2}$ . High resolution x-ray diffraction (HRXRD) was used to characterize the crystalline quality and buffer leakage characteristics were measured by applying 1000 V bias voltage between two adjacent pads separated by a distance of 100 μm. Table I compares the crystalline quality and buffer leakage characteristics of the three typically used buffer structures on sapphire. The GaN/AlN buffer can provide a low threading dislocation (TD) density of  $3.2 \times 10^8 \text{ cm}^{-2}$  while maintaining a low buffer leakage of 21 nA. For the HR GaN buffer and HQ GaN buffer using LT-GaN as nucleation layer, however, low TD density and low buffer leakage cannot be achieved simultaneously.

After the HEMT growth and characterization, a 200 nm  $\text{SiO}_2$  layer was deposited by plasma-enhanced chemical vapor deposition (PECVD), patterned by photolithography and buffered oxide etch (BOE) for selective growth of the LED part. The top 200 nm AlGaN/GaN stack was selectively removed by inductively coupled plasma (ICP) etching, exposing the GaN buffer underneath and the sidewall GaN channel to be connected to the LED overgrowth. Afterwards, SAG of the LED structure was performed in the exposed region. The LED consisted of 1.5 μm n-type GaN, five periods of  $\text{In}_{0.1}\text{Ga}_{0.9}\text{N}/\text{GaN}$  multi-quantum wells (MQWs) with 3 nm-thick wells and 12 nm-thick barriers, followed by a 15 nm p-type  $\text{Al}_{0.15}\text{Ga}_{0.85}\text{N}$  and a 170 nm p-type GaN layer.

After the LED regrowth, the  $\text{SiO}_2$  regrowth mask was completely stripped after immersion in BOE for one hour. Mesa definition for the LED- and the HEMT- parts was performed separately by ICP etching. The source ohmic contact of the HEMT was formed by e-beam evaporation of Ti/Al/Ni/Au and rapid thermal annealing (RTA) at 850 °C for 30 s in  $\text{N}_2$  ambient. Afterwards, a Ni/Au current spreading layer and a Ti/Al/Ti/Au p-electrode of the LED were evaporated. Finally, Ni/Au gate metallization was realized for the HEMT. The 2DEG channel of the HEMT was connected laterally to the n-type GaN electrode of the LED through intimate contact of the epi-layers, and no external metal-interconnection was needed. A schematic of the finished HEMT-LED device is shown in Fig. 1. Electrical properties were measured by on-wafer probing and electroluminescence properties were collected in an integrating sphere at room temperature.

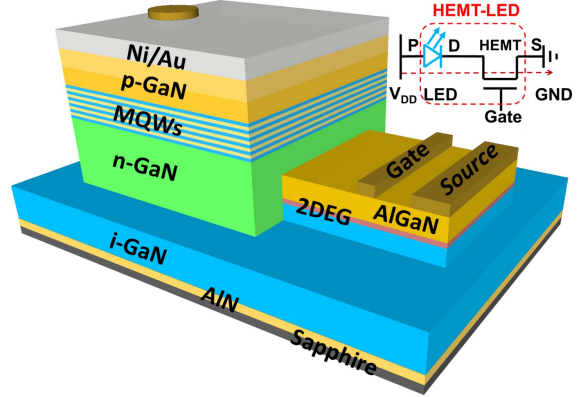


Fig. 1. Schematic of the metal-interconnect-free HEMT-LED device using the GaN/AlN buffer.

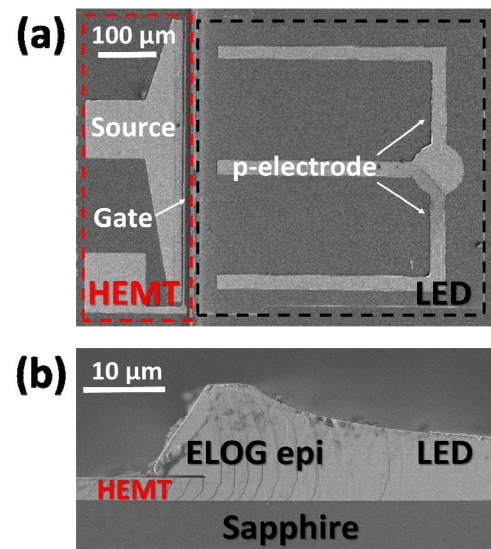
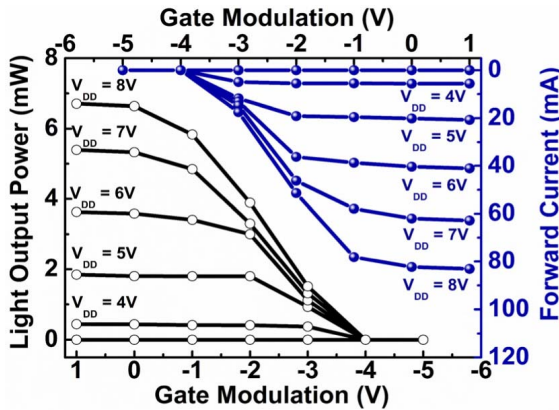
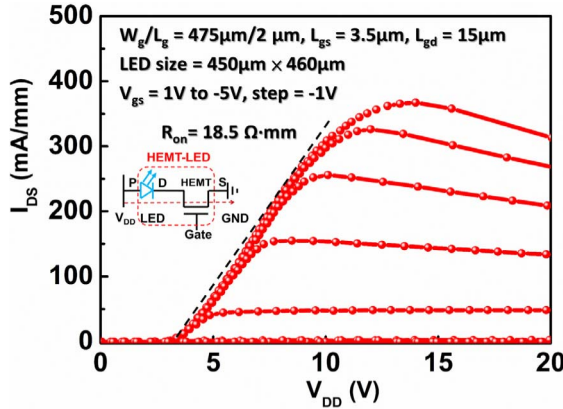


Fig. 2. (a) Top view SEM image, and (b) Cross-sectional view SEM image of the integrated HEMT-LED.

### III. RESULTS AND DISCUSSION

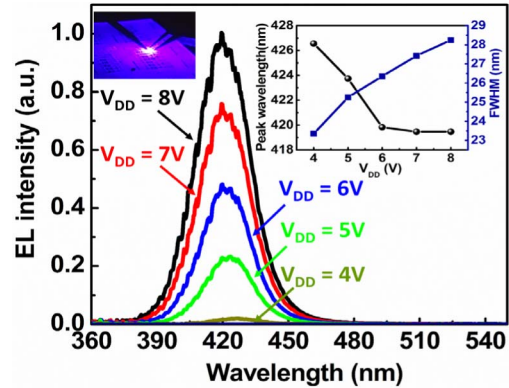
Fig. 2 (a) is a top view scanning electron microscopic (SEM) image of an integrated HEMT-LED. The device is composed of a HEMT with a  $W_g/L_g$  ratio of 475 μm/2 μm and an LED with a light-emitting area of 450 μm × 460 μm. The HEMT/LED footprint ratio used in this work is ~ 0.27, which was based on a layout design considering the direct current (DC) driving capability of the HEMT and the operation current density of the LED. Fig. 2 (b) shows a cross-sectional view of the fully processed HEMT-LED near the SAG interface. The seamless contact between the 2DEG channel of the HEMT and the n-type GaN layer of the LED is the key factor for a reduced interconnect resistance, as analyzed in Ref [10]. In addition, elimination of the metal interconnect helps to reduce related parasitic inductance and capacitance, thereby mitigating power loss during fast switching. We observe an epitaxial lateral overgrowth (ELOG) region, crawling across the  $\text{SiO}_2$  regrowth mask and forming a 60° angle, due to an enhanced growth rate near the regrowth mask. An air void or residue oxide between the ELOG LED epi and the bottom



HEMT epi after stripping of the  $\text{SiO}_2$  mask in BOE does not affect any electrical characteristics of the devices.

Fig. 3 plots the I-V characteristics of the integrated HEMT-LED device as a function of the supply voltage ( $V_{DD}$ ) of the HEMT-LED device and the gate voltage ( $V_{GS}$ ) of the HEMT. The current flow through the HEMT-LED can be well modulated by the  $V_{GS}$  of the HEMT. A maximum current density ( $I_{dss}$ ) of 370 mA/mm was measured from the integrated HEMT-LED, which corresponds to a maximum 180 mA driving current for the light-emitting part. The specific on-state resistance of the integrated HEMT-LED is  $18.5 \Omega\cdot\text{mm}$  by linear extrapolation. The turn on voltage of around 3 V is due to the LED connected in series with the driving transistor. Other than the voltage shift, the integrated HEMT behaves similarly to a stand-alone HEMT from the same wafer.  $I_{ds}$  decreases gradually beyond saturation, which is attributed to a thermally induced mobility degradation [13], [14].

Fig. 4 illustrates the fully modulated light output power (LOP) of the integrated HEMT-LED by  $V_{GS}$  and  $V_{DD}$  through the injection current from the driving transistor. No light emission was observed while the HEMT is pinched off with a  $V_{GS}$  below  $-4$  V. With increasing  $V_{GS}$ , a nearly linear modulation of the LOP can be observed before saturation. Note that the saturation of the LOP appears at a more negative  $V_{GS}$  when the HEMT-LED is biased at a



smaller  $V_{DD}$ . Besides the gate modulation, the brightness of the HEMT-LED can also be tuned by  $V_{DD}$ . Furthermore, the LOP of the integrated HEMT-LED can reach  $\sim 7$  mW at an injection current of  $\sim 80$  mA ( $V_{DD} = 8$  V and  $V_{GS} = 1$  V), which is a dramatic improvement compared to the previously reported 2 mW at 80 mA injection current [10]. The improvement can be attributed to improved crystalline quality with the optimal GaN/AlN buffer structure. Further enhanced brightness of the integrated LED can be achieved by a number of technologies such as epitaxial structure design, surface roughening, advanced packaging and et al.

Electroluminescence (EL) spectra from the integrated HEMT-LED modulated by  $V_{DD}$  at a gate bias of 1 V are shown in Fig. 5. The inset shows the violet light emission from the three-terminal HEMT-LED device. As  $V_{DD}$  increased, the EL peak intensity was enhanced, indicating control of the LED brightness by  $V_{DD}$ . Moreover, blueshift of the peak wavelength and FWHM broadening of the EL spectrum were observed with increased  $V_{DD}$ . This can be attributed to the Coulomb screening of the piezoelectric field induced quantum-confined Stark effect and band-filling effect of carriers in quantum wells with increased injection current modulated by  $V_{DD}$  [15].

The off-state breakdown characteristics of the integrated HEMT-LED at forward bias and reverse bias were measured, according to the equivalent circuit shown in Fig. 6 (a). The integrated HEMT-LED is treated as a three-terminal device in the dash-lined box. The external terminals are labelled as P, S (source), and G (gate), respectively. Since the 2DEG channel of the HEMT and the n-type GaN of the LED were internally connected during selective area growth, we define the virtual D (drain) terminal to be at the HEMT/LED edge. The G-to-S distance ( $L_{GS}$ ) is  $3.5 \mu\text{m}$  and G-to-D distance ( $L_{GD}$ ) is  $15 \mu\text{m}$ . The breakdown voltage is defined as the measured voltage when the off-state current density reaches 1 mA/mm. At forward  $V_{DD}$  bias, a breakdown voltage exceeding 530 V can be achieved for the integrated HEMT-LED, while at reverse bias conditions, the breakdown voltage of the HEMT-LED is around 270 V, as shown in Fig. 6 (b). The high breakdown performance of the integrated HEMT-LED is mainly attributed to the high resistivity GaN/AlN buffer underneath.

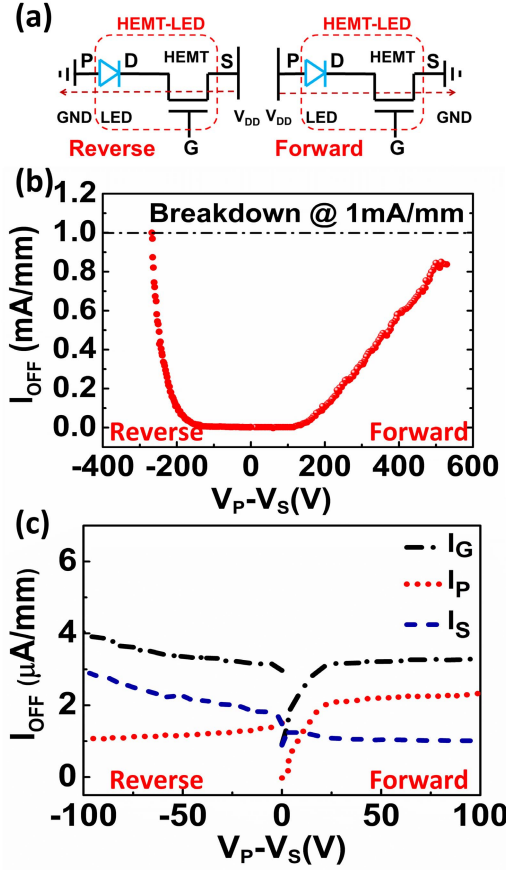


Fig. 6. (a) Equivalent circuits for forward and reverse bias measurement, (b) off-state breakdown, and (c) off-state leakage characteristics of the integrated HEMT-LED at forward and reverse bias.

To explain the difference in the breakdown voltage at forward and reverse bias conditions, the off-state leakage current path through the integrated HEMT-LED was analyzed, as shown in Fig. 6 (c). At forward bias, the on-state LED has negligible specific on-resistance and the breakdown behavior of the HEMT-LED is similar to a typical HEMT, in which the P-to-G leakage path dominates and the breakdown first occurs at the gate terminal. At reverse bias, the dominant off-state leakage current flows from the S terminal to the G terminal. As a result, the smaller L<sub>GS</sub> of 3.5  $\mu$ m results in a reduced breakdown voltage. The breakdown performance at reverse bias conditions can be further improved with an optimized layout design.

#### IV. CONCLUSION

In conclusion, we achieved a laterally integrated HEMT-LED with an optimized GaN/AlN buffer structure without compromising the performance of either the LED or HEMT. The enhanced light output power from

the integrated LED is attributed to improved crystalline quality and the record-high breakdown characteristics of the integrated HEMT-LED are due to the high resistivity of the GaN/AlN buffer used in this work. This is the first time a monolithically integrated HEMT-LED with such superior performance has been demonstrated, bringing great potential for a variety of applications, such as smart lighting or visible light communication by efficient voltage-controlled ICs.

#### REFERENCES

- [1] F. G. Kalaitzakis, E. Iliopoulos, G. Konstantinidis, and N. T. Pelekanos, "Monolithic integration of nitride-based transistor with light emitting diode for sensing applications," *Microelectron. Eng.*, vol. 90, pp. 33–36, Feb. 2012.
- [2] K. M. Lau *et al.*, "Cost-effective and eco-friendly LED system-on-a-chip (SoC)," in *Proc. 10th China Int. Forum Solid State Lighting (ChinaSSL)*, Beijing, China, Nov. 2013, pp. 235–238.
- [3] J. W. Chung, W. E. Hoke, E. M. Chumbes, and T. Palacios, "AlGaN/GaN HEMT with 300-GHz  $f_{max}$ ," *IEEE Electron Device Lett.*, vol. 31, no. 3, pp. 195–197, Mar. 2010.
- [4] Z. Li, J. Waldron, T. Detchprohm, C. Wetzel, R. F. Karlicek, Jr., and T. P. Chow, "Monolithic integration of light-emitting diodes and power metal-oxide-semiconductor channel high-electron-mobility transistors for light-emitting power integrated circuits in GaN on sapphire substrate," *Appl. Phys. Lett.*, vol. 102, no. 19, pp. 192107-1–192107-3, May 2013.
- [5] Z. Li *et al.*, "High temperature characteristics of monolithically integrated LED and MOS-channel HEMT in GaN using selective epi removal," *Phys. Status Solidi A*, vol. 212, no. 5, pp. 1110–1115, May 2015.
- [6] Y.-J. Lee *et al.*, "Monolithic integration of GaN-based light-emitting diodes and metal-oxide-semiconductor field-effect transistors," *Opt. Exp.*, vol. 22, pp. A1589–A1595, Oct. 2014.
- [7] Z. J. Liu, T. Huang, J. Ma, C. Liu, and K. M. Lau, "Monolithic integration of AlGaN/GaN HEMT on LED by MOCVD," *IEEE Electron Device Lett.*, vol. 35, no. 3, pp. 330–332, Mar. 2014.
- [8] Z. Liu, J. Ma, T. Huang, C. Liu, and K. M. Lau, "Selective epitaxial growth of monolithically integrated GaN-based light emitting diodes with AlGaN/GaN driving transistors," *Appl. Phys. Lett.*, vol. 104, no. 9, pp. 091103-1–091103-3, Mar. 2014.
- [9] C. Liu, Z. Liu, T. Huang, J. Ma, and K. M. Lau, "Improved breakdown characteristics of monolithically integrated III-nitride HEMT-LED devices using carbon doping," *J. Cryst. Growth*, vol. 414, pp. 243–247, Mar. 2015.
- [10] C. Liu, Y. Cai, Z. Liu, J. Ma, and K. M. Lau, "Metal-interconnection-free integration of InGaN/GaN light emitting diodes with AlGaN/GaN high electron mobility transistors," *Appl. Phys. Lett.*, vol. 106, no. 18, pp. 181110-1–181110-4, May 2015.
- [11] S. Das Bakshi, J. Sumner, M. J. Kappers, and R. A. Oliver, "The influence of coalescence time on unintentional doping in GaN/sapphire," *J. Cryst. Growth*, vol. 311, no. 2, pp. 232–237, Jan. 2009.
- [12] T. Zhu and R. A. Oliver, "Unintentional doping in GaN," *Phys. Chem. Chem. Phys.*, vol. 14, no. 27, pp. 9558–9573, May 2012.
- [13] Y. F. Wu *et al.*, "High power AlGaN/GaN HEMTs for microwave applications," *Solid-State Electron.*, vol. 41, no. 10, pp. 1569–1574, Oct. 1997.
- [14] S. Arulkumaran, T. Egawa, H. Ishikawa, and T. Jimbo, "High-temperature effects of AlGaN/GaN high-electron-mobility transistors on sapphire and semi-insulating SiC substrates," *Appl. Phys. Lett.*, vol. 80, no. 12, pp. 2186–2188, Jan. 2002.
- [15] S. Chichibu, T. Azuhata, T. Sota, and S. Nakamura, "Spontaneous emission of localized excitons in InGaN single and multiquantum well structures," *Appl. Phys. Lett.*, vol. 69, no. 27, pp. 4188–4190, 1996.